

PAINTING WITH MUSIC

by

Weijian Zhou

A thesis submitted in conformity with the requirements
for the degree of Master of Applied Science and Engineering
Graduate Department of Electrical and Computer Engineering
University of Toronto

© Copyright 2015 by Weijian Zhou

Abstract

Painting with Music

Weijian Zhou

Master of Applied Science and Engineering

Graduate Department of Electrical and Computer Engineering

University of Toronto

2015

In this paper, we described a small area sound localization system with two microphone arrays. We evaluated different array architectures and demonstrated that a two array system outperforms a single array system of similar physical dimension. The proposed system localizes in 80 milliseconds and achieved an average error of less than 3 cm for both point localization and movement tracking in a local one meter by one meter region.

Contents

1	Introduction	1
2	Background	3
2.1	ILD	3
2.2	LTM	5
2.3	TDOA	5
3	Array Architecture	10
4	System Setup	16
5	Experiment	20
5.1	Setup	20
5.1.1	Point localization	20
5.1.2	Movement tracking	20
5.2	Results	22
5.2.1	Point localization	22
5.2.2	Movement tracking	28
6	Conclusion	37
	Bibliography	37

Chapter 1

Introduction

Accurate indoor localization allows creation of novel applications with surrounding awareness that uses position and movement information as input. One application is to allow users to draw with music without physically touching the computer. Another example is to build AI games with physical pieces such as toy car racing where the computer controls some of the toy cars. In this work, we aim to build such a source localization system that is portable, inexpensive, yet reasonably accurate for localization in a small area.

Global Positioning System (GPS) is the prevailing technology used for outdoor localization. Commercial grade GPS has an average error of a few meters, depending on the size and quality of the receiver [1]. While accuracy in this range is good for many applications including driving navigation and vehicle tracking, it does not provide enough precision for local movement tracking. Ultrasound based indoor localization approaches on the other hand, have achieved sub-centimeter accuracy [4]. However, ultrasound systems require the use of expensive transducers.

Bluetooth and Wi-Fi based technologies have gained popularity in indoor positioning recently, mainly due to the widespread deployment of bluetooth tags and Wi-Fi stations in public spaces. In these systems, signal strength received from different base stations

are used for the estimation of the device location. However, their reported accuracy are in the range of 1 to 5 meters [2, 3], which is not enough for local movement tracking.

In this project, we have built a localization system with reasonably high precision for small area using microphone arrays that localize typical audio sources. Our system is built with inexpensive electret microphones mounted on portable frames. Users can interact with our system using any device that has audio output such as a mobile phone.

In this paper, we first discussed in Chapter II some prior relevant research and approaches in sound localization. In Chapter III, we evaluated different array architectures and their impact on localization accuracy. We demonstrated that a two array system outperforms a single array system of similar physical dimension. In Chapter IV, we presented the chosen architecture along with hardware details. Finally, experiment details and results were presented in Chapter V.

Chapter 2

Background

Acoustic localization has been researched extensively in the literature. Localization techniques can be broadly categorized into Interaural Level Difference (ILD), Location Template Matching (LTM), and Time Difference of Arrival (TDOA) based approaches.

2.1 ILD

ILD techniques rely on the observation that signal intensity decays as the distance to the microphone increases. A microphone closer to the signal source would receive the signal with higher intensity than a microphone farther away. With multiple microphones, it is possible to infer the source location by comparing the signal intensity received at different microphones. Human's auditory system has used ILD cues to infer source direction [6], and this technique is most effective to localize high frequency sources, because they don't diffract effectively around the listener's head and produce a significant intensity difference.

Let $s(t)$ denote the audio signal. The received signal $\bar{s}(t)$ at microphone i can be modeled as:

$$\bar{s}_i(t) = \frac{s(t)}{d_i} + \delta_i(t)$$

where d_i is the distance between the audio source and microphone i , and $\delta_i(t)$ represents Gaussian noise. The energy received at microphone i is:

$$E_i = \int \bar{s}_i(t)^2 dt \quad (2.1)$$

$$= \frac{1}{d_i^2} E_s + E_{\sigma_i} \quad (2.2)$$

It shows that the energy decays with the square of the distance. With two microphones, not considering the noise $\delta_i(t)$, energy received at both microphones has to satisfy equation 2.2:

$$E_1 d_1^2 = E_2 d_2^2 \quad (2.3)$$

$$\frac{E_1}{E_2} = \frac{d_2^2}{d_1^2} \quad (2.4)$$

It can be shown that, on a 2D plane, points satisfy equation 2.4 form a circle when $E_1 \neq E_2$ and form a line when $E_1 = E_2$ [5]. With two microphones all points on this curve generate the same energy ratio and can not be distinguished from each other. Multiple approaches have been investigated to eliminate this ambiguity. [5] employed multiple microphones and used the intersection of circles from each microphone pair to estimate the source location. [6] combined ILD with Interaural Time Difference to estimate the source direction (i.e azimuth).

ILD approach relies on the accurate measurement of the received energy ratio between microphone pairs. Any obstacle object between the sound source and any microphone would produce a significant distortion in the measured energy ratio. We find this approach to be too restrictive for our system, since in an interactive system we can not control whether or not the user places any obstacle between the sound source and the microphones.

2.2 LTM

In LTM based approaches, acoustic templates acquired from different locations are first stored in the system during a “training” phase. Localization can be performed by comparing the incoming waveform with the stored templates, and the location with the best matching template is chosen as the output. Different ways of extracting templates from raw acoustic source and different similarity measures have been investigated in the past.

[8] and [9] investigated using max value from cross-correlation as a similarity measure to localize user taps on interactive surfaces. [10] used L2 distance in the Linear Predictive Coding coefficient space as a similarity measure to localize taps on surfaces. [11] further explored accuracy improvement by using multiple templates for each location and speed improvement by merging multiple templates into one representative template.

The requirement of having a template for each location to be detected makes this approach too restrictive for our project, since we want the localization to be continuous in a 2D region. Moreover, the need to recalibrate all locations during setup is too cumbersome for the end users in a portable system. Therefore, our main focus will be on TDOA based approaches.

2.3 TDOA

TDOA approaches exploit the difference of arrival time between the acoustic source and two fixed microphones on the plane. It can be easily shown that the acoustic sources with the same TDOA to two fixed microphones on the plane form a hyperbola. When you have more than two microphones, each pair would give a different hyperbola. The intersection of all the hyperbolas marks the source location. TDOA approaches rely on accurate estimates of arrival time differences between microphones.

In [12], authors used eight microphones mounted on the corners of a ping pong table to localize points where the ball hits the table. They used a threshold to determine the

arrival time of acoustic signal. This approach works well in noise free environment but the performance degrades with background noise. Their approach also suffers from dispersive deflections that arrive before the main wavefront of the acoustic signal. To make it more robust, authors in [17] and [18] extracted descriptive parameters for each significant peak(e.g., peak height, width, mean arrival time). The algorithm then used extracted parameters to predict arrival time with a second order polynomial, the parameters of which were fitted during calibration at fixed locations.

Cross-correlation has also been used to measure signal arrival time differences[13, 14, 16]. Cross correlation is a measure of similarity between two signals. For real valued signals $x_1(t)$, $x_2(t)$ a time shift τ :

$$\text{xcorr}_{x_1,x_2}(\tau) = \int_{-\infty}^{\infty} x_1(t)x_2(t + \tau)dt \quad (2.5)$$

We can take Fourier Transform on both sides of equation 2.5:

$$\mathcal{F}\{\text{xcorr}_{x_1,x_2}(\tau)\} = X_1(\omega)X_2(-\omega) \quad (2.6)$$

$$= X_1(\omega)X_2(\omega)^* \quad (2.7)$$

Where $X_1(\omega)$ and $X_2(\omega)$ are the Fourier Transforms of $x_1(t)$ and $x_2(t)$. We can retrieve the cross-correlation result in time domain by taking inverse Fourier transform:

$$\text{xcorr}_{x_1,x_2}(\tau) = \int_{-\infty}^{\infty} X_1(\omega)X_2(\omega)^*e^{j\omega\tau}d\omega \quad (2.8)$$

The arrival time difference t_0 is time shift τ that maximizes 2.8:

$$t_0 = \arg \max_{\tau} \text{xcorr}_{x_1,x_2}(\tau) \quad (2.9)$$

The benefits of calculating cross-correlation in the frequency domain as shown in

equation 2.8 are two folds. The first benefit is to speedup the calculation. Calculating cross-correlation using equation 2.5 requires multiplying and summing the two signal vectors for each time shift τ . With discrete signals of length n , it will take $O(n^2)$ number of calculations. Doing the same calculation in frequency domain, we need to transform the signal into frequency domain, multiple and sum the two transformed signal vectors once and then transform the result back to the time domain. Transforming a signal from time domain to frequency domain and back can be done efficiently with Fast Fourier Transform (FFT) and Inverse Fast Fourier Transform (IFFT), and the amount of calculation needed is $O(n \log n)$. Multiply and sum the transformed signal vectors takes another $O(n)$. Therefore, the total calculation required to calculate cross-correlation using Fourier transform is $O(n \log n)$, which is asymptotically faster than calculating in the time domain.

The second benefit of formulating cross correlation in frequency domain is that it provides a unified framework to prefilter the signals. Cross-correlation with prefiltering is known as *generalized cross correlation (GCC)*. Different prefiltering approaches have been investigated to improve arrival time difference estimation [19, 20, 21]. Under the GCC framework, the arrival time difference t_0 between two signals $x_1(t)$ and $x_2(t)$ is estimated as:

$$t_0 = \arg \max_{\tau} R_{x_1 x_2}(\tau) \quad (2.10)$$

$$R_{x_1 x_2}(\tau) = \int_{-\infty}^{\infty} W(\omega) X_1(\omega) X_2^*(\omega) e^{j\omega\tau} d\omega \quad (2.11)$$

$W(\omega)$ provides a way to prefilter signals passed to the cross correlation estimator. We focused on three ways of prefiltering the signal:

GCC $W(\omega) = 1$. No prefiltering is done. This is unfiltered normal cross correlation.

GCC_PPHAT $W(\omega) = \frac{1}{|X_1(\omega)X_2^*(\omega)|}$. Each frequency is divided by its magnitude. Only phase information contributes to delay estimation.

GCC_PHAT_SQRT $W(\omega) = \frac{1}{|X_1(\omega)X_2^*(\omega)|^{0.5}}$. This is somewhere between GCC and GCC_PHAT. Part of magnitude information is included in arrival time difference estimation.

To see the reasoning behind different prefiltering approaches, we separate the magnitude part from the phase part of $X_1(\omega)$ and $X_2(\omega)$ in Equation 2.11:

$$R_{x_1x_2}(\tau) = \int_{-\infty}^{\infty} W(\omega)|X_1(\omega)||X_2(\omega)|e^{j(\omega\tau - (\angle X_2(\omega) - \angle X_1(\omega)))} d\omega \quad (2.12)$$

$$= \underbrace{\int_{-\infty}^{\infty} W(\omega)|X_1(\omega)||X_2(\omega)|}_{\text{weighting}} \underbrace{\cos(\omega\tau - (\angle X_2(\omega) - \angle X_1(\omega)))}_{\text{phase error}} d\omega \quad (2.13)$$

We can look at the real part of equation 2.12 only since both $x_1(t)$ and $x_2(t)$ are real valued signals. When $\dot{\tau}$ is the true arrival time difference between $x_1(t)$ and $x_2(t)$, $\omega\dot{\tau} - (\angle X_2(\omega) - \angle X_1(\omega)) = 0$, and $\cos(\omega\dot{\tau} - (\angle X_2(\omega) - \angle X_1(\omega))) = 1$. When $\dot{\tau}$ differs from the true arrival time difference, $\cos(\omega\dot{\tau} - (\angle X_2(\omega) - \angle X_1(\omega))) < 1$. Therefore, $\cos(\omega\tau - (\angle X_2(\omega) - \angle X_1(\omega)))$ can be seen as a measure of the phase error, and $W(\omega)|X_1(\omega)||X_2(\omega)|$ describes how the error should be weighted at each frequency. The TDOA estimator essentially sums the weighted phase error at each frequency.

Without any prefiltering (i.e $W(\omega) = 1$), the estimator weighs the phase error at each frequency by the magnitude of the signal at that frequency. In this weighting scheme, phase error at frequencies with higher magnitudes are penalized more compared to frequencies with a lower magnitude. This weighting is appropriate if there is only one source present, since frequencies with higher magnitude have higher Signal to Noise Ratio (SNR). It makes sense to place higher weights at frequencies with higher SNR, since low SNR regions can be dominated by noise.

However, with multiple sources, the source with the highest magnitude will dominate the phase error estimation, but there is no particular reason to assign a higher weight to the source with the highest volume. All sources should contribute equally in the phase error estimation. In GCC_PHAT, $W(\omega)$ is set to $\frac{1}{|X_1(\omega)||X_2(\omega)|}$. In effect it ignores

the signal magnitude and weighs phase errors uniformly across frequencies. Since the phase error at every frequency is weighted equally, this technique will suffer from error accumulation if the source has a lot of low power regions in the frequency domain.

In GCC_PHAT_SQRT, $W(\omega)$ is set to $\frac{1}{(|X_1(\omega)|\|X_2(\omega)\|)^{0.5}}$. Phase error weighting at each frequency still depends on the signal strength at that frequency, but the dependency is much weaker than that in unfiltered GCC. On the other hand, this weighting scheme doesn't go to the other extreme of completely ignoring signal strength information as does in GCC_PHAT. This approach represents a balance between unfiltered GCC and GCC_PHAT.

Chapter 3

Array Architecture

As was mentioned in the previous chapter, points with the same TDOA to two fixed locations form a hyperbola on a 2D plane. However, in practical systems we can only measure TDOA up to a precision. Therefore we look at all points with difference of distance close to some target value within measurement error ϵ . This ϵ represents accuracy on the measurement of difference of distances, and in practice it is related to sampling rate and estimation techniques. In this chapter we evaluate the impact of difference of distance estimation on localization accuracy.

To see how precision affects localization accuracy, we simulated two microphones placed at: $M_1 : (x = -10 \text{ cm}, y = 0 \text{ cm})$ and $M_2 : (x = 10 \text{ cm}, y = 0 \text{ cm})$. A test sound source is emitted at point P which is 50 centimeters away from the origin $(0, 0)$. Let $2a$ denote the TDOA between P and two microphones:

$$2a = \frac{PM_1 - PM_2}{340 \text{ m/s}}$$

where 340 m/s is used as the speed of sound. Assuming a sampling rate of 34 KHz, fig 3.1 shows the region R where all points have TDOA close to $2a$ s within one sample difference:

$$R = \{\hat{P} : \left| \frac{(\hat{P}M_1 - \hat{P}M_2)}{340 \text{ m/s}} - 2a \right| < \frac{1}{2} \text{ samples}\}$$

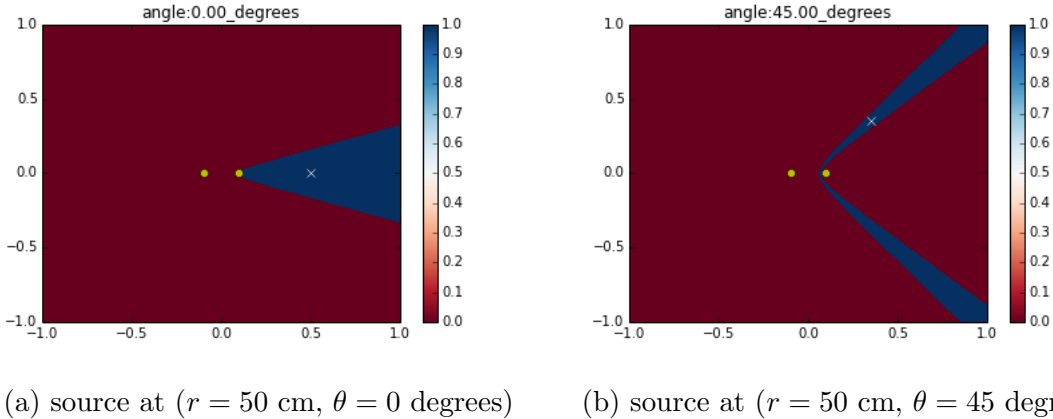


Figure 3.1: Uncertainty region. Yellow dots represent microphones' locations and the white dot represents the location of the source.

Intuitively, points in R have TDOA to two microphones very similar to each other. Looking at fig 3.1, we can still see that R has the shape of a hyperbola, but with an uncertainty region around it. The thickness of the uncertainty region is not uniform around the hyperbola, the farther away the point is, the larger the uncertainty region becomes. This indicates for the same delta distance movement it will generate smaller TDOA change when the source is farther away from the array. The size of the uncertainty region is also angle dependent: points closer to the line connecting microphones have larger region compared to points close to the line bisecting microphones.

This can also be seen analytically. Assuming two microphones are placed on the x-axis at $M_1 : (-c, 0)$ and $M_2 : (c, 0)$. All points $P : (x, y)$ with difference of distance $|PM_1 - PM_2| = 2a$ satisfies:

$$\frac{x^2}{a^2} - \frac{y^2}{c^2 - a^2} = 1 \quad (3.1)$$

To see how the difference of distance changes with respect to source location, we can expand the equation and find the partial differential $\frac{\partial a}{\partial x}$:

$$\frac{\partial a}{\partial x} = \frac{x(c^2 - a^2)}{a(x^2 + y^2 + c^2) - 2a^3} \quad (3.2)$$

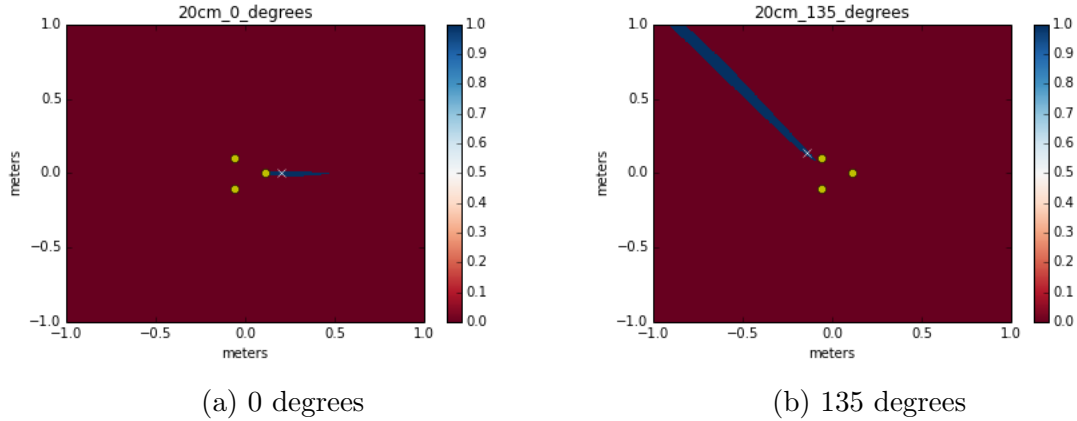


Figure 3.2: Uncertainty region. Microphones are at the vertices of a 20cm equilateral triangle. The source is 20cm away from the array.

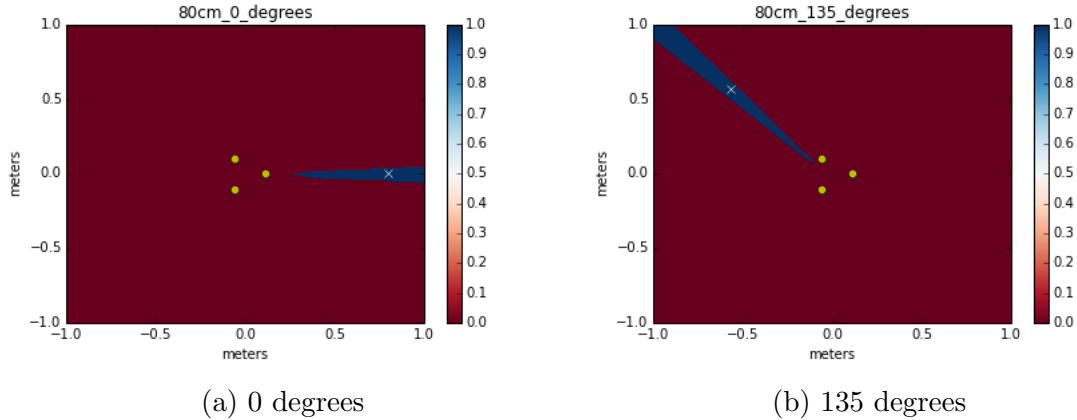


Figure 3.3: Uncertainty region. Microphones are at the vertices of a 20cm equilateral triangle. The source is 80cm away from the array.

Since all points in equation 3.2 must lie on the hyperbola, we can substitute 3.1 into 3.2:

$$\frac{\partial a}{\partial x} = \frac{c^2 - a^2}{\frac{c^2}{a}x - \frac{a^3}{x}} \quad (3.3)$$

The denominator of equation 3.3 increases monotonically as $|x|$ increases, which indicates $\frac{\partial a}{\partial x}$ decreases as we move farther away along the hyperbola. The same distance move δx would generate smaller change in difference of distance a when the source is farther away from the microphones.

With more than two microphones, each pair of microphones generates a hyperbolic re-

gion and localization becomes finding the intersection of hyperbolic regions. The smaller the intersection region, the better the localization accuracy. To see how accuracy changes with array placement and sound source location, three microphones are placed at the three vertices of a 20 cm equilateral triangle. An audio source is placed at 20 cm away from the center of the array. Fig 3.2 shows the intersection of regions for 2 different placement of the sound source. It can be seen that accuracy decreases when sound source becomes close to the line connecting any two microphones. This observation is consistent with the two microphone case, since points close to lines connecting microphones have a larger uncertainty region.

To see how sound source distance affects localization accuracy, the same simulation is carried out with the sound source moved from 20 cm to 80 cm away from the center of the array. Results are presented in fig 3.3. Comparing with fig 3.2, accuracy decreases as the distance to the array increases. This is also consistent with our observation in 2 microphone case where sources farther away would result in larger uncertainty region.

Each microphone pair generates a hyperbolic region, and the source location is in the intersection of these regions. The area of the intersection region is a measure of the localization accuracy: the smaller the area, the more certain we are about the source location. To evaluate an array's accuracy in a region, we can place sound source at predetermined grid points in the region and look at the intersection area for each tested point in the grid. The center location of the intersection region can be used as the localization estimate to calculate localization error. Results for a few different microphone array configurations are presented in fig 3.4.

Fig 3.4a shows the accuracy when microphones are placed at the three vertices of a 20 cm equilateral triangle. The region inside the array has good accuracy. However, for regions along the line connecting any two microphones, the accuracy drops significantly. The average error across the region is 18.6 cm.

To evaluate how adding one microphone (without increasing the array size) improves

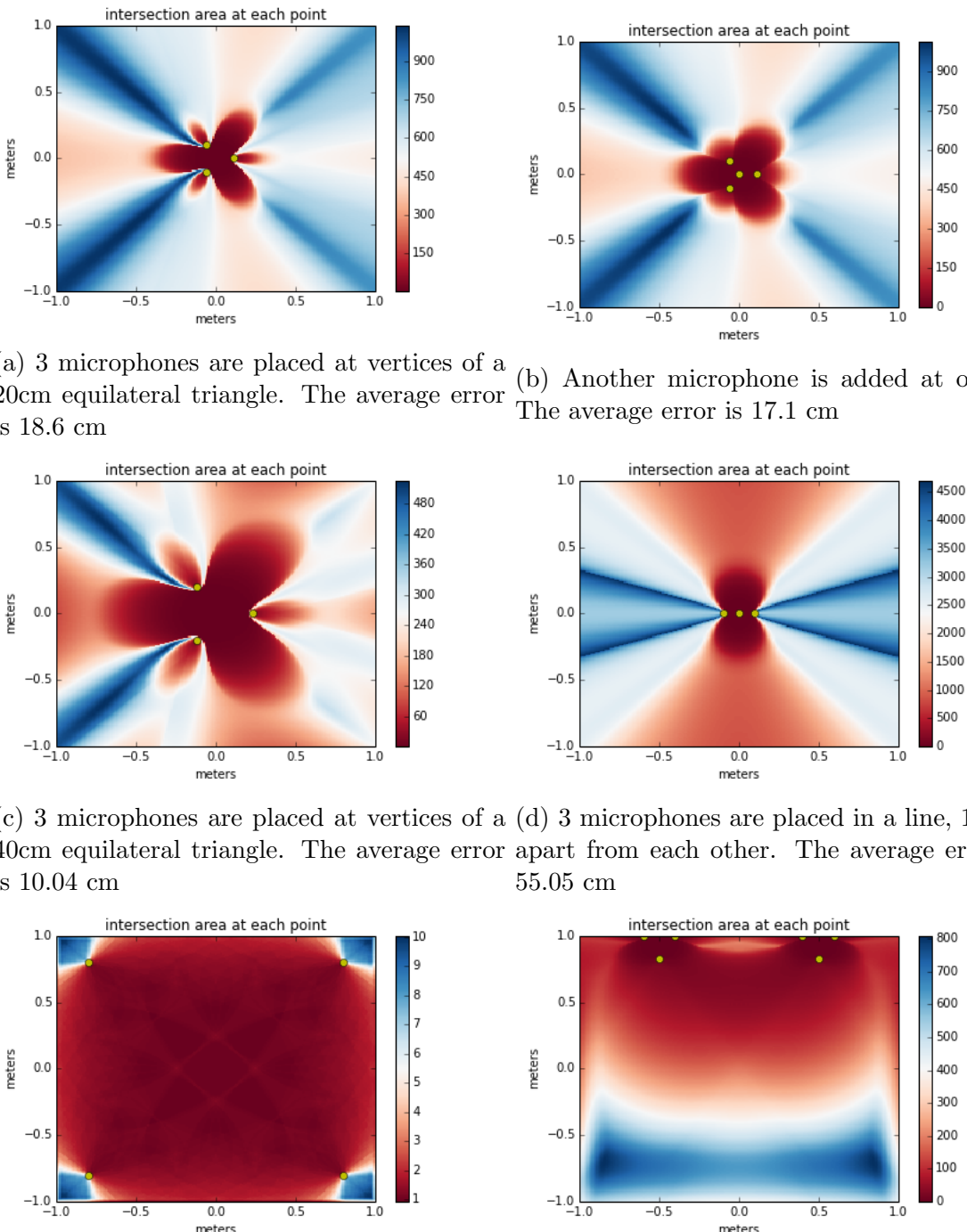


Figure 3.4: Error heatmap for different array configurations. The heatmap scale is the intersection area measured in cm^2

accuracy, another microphone is added to the array at $(0, 0)$. Result is presented in fig 3.4b. Addition of the new microphone only slightly improved the accuracy around the array region. The average error dropped from 18.6 cm to 17.1 cm. Regions near lines connecting microphones still have significantly larger uncertainty region.

To evaluate the array size's impact on accuracy, the size of the original array (as in fig 3.4a) is increased by a factor of 2. The result is presented in fig 3.4c. The overall uncertainty area decreased across the region. The average error improved to 10.04 cm.

In fig 3.4d, three microphones are placed 10 cm apart from each other on the x-axis. Error heatmap shows high uncertainty on the x axis, and the overall accuracy is not as good as that with three microphones placed in a triangle. The average error is 55.05 cm.

To further increase the distance between microphones, we placed four microphones at four corners of the region. Fig 3.4e shows the result. With this configuration, accuracy is consistently good across the region. The average error is 0.05 cm. However, placing microphones far apart at corners of the region requires accurate placement of all four individual microphones. The system is less portable compared to small arrays with microphones near each other. Placing microphones far apart from each other also causes problems in TDOA estimation, because sampling of microphones in the same array requires synchronized clock.

To avoid the need to accurately place microphones at far distances (as required by fig 3.4e), we explored configuration with two arrays. Two 3 microphone array are placed 1 meter apart and the result is presented in fig 3.4f. The result indicates that this configuration has good accuracy when source is close to the arrays. Accuracy decreases as sound source moves outside of the one meter by one meter region. The average error is 2.60 cm.

With the simulation results, we decided to build the two array system as described in fig 3.4f. The setup is reasonably portable (compared to fig 3.4e), while at the same time having significantly better accuracy compared to one array systems.

Chapter 4

System Setup

The end system has two arrays, each with three microphones mounted on the vertices of a 20 cm equilateral triangle. A micro-controller is attached to one of the vertices. Fig 4.1 shows a picture of the array setup. The micro-controller used in this project is *teensy 3.1*, which has 64k RAM memory and the ADC is capable of sampling at 500kHz [14, 15]. In this project, the micro-controller collects microphone data on all three channels for 12 milliseconds and then sends the recorded data to a computer through the USB port for localization.

To handle the uncertainty in TDOA estimation, instead of using point estimate that maximizes equation 2.10, we take the cross-correlation output(equation 2.11) as a measure of the likelihood of different arrival time differences. For each microphone array, we build a heatmap for the region. The intensity at each point represents the likelihood of it being the source. For each point on the grid, the theoretical TDOA to each microphone pair can be precomputed. Then the heatmap can be generated by going through points on the grid and performing a lookup using equation 2.11. With three microphones m_1 , m_2 , and m_3 , there are three microphone pairs: m_1m_2 , m_1m_3 , and m_2m_3 . The theoretical TDOA from each location (x, y) to each microphone pair is precomputed and stored in $D_{m_1,m_2}(x, y)$, $D_{m_1,m_3}(x, y)$, and $D_{m_2,m_3}(x, y)$. Then the likelihood map $L(x, y)$

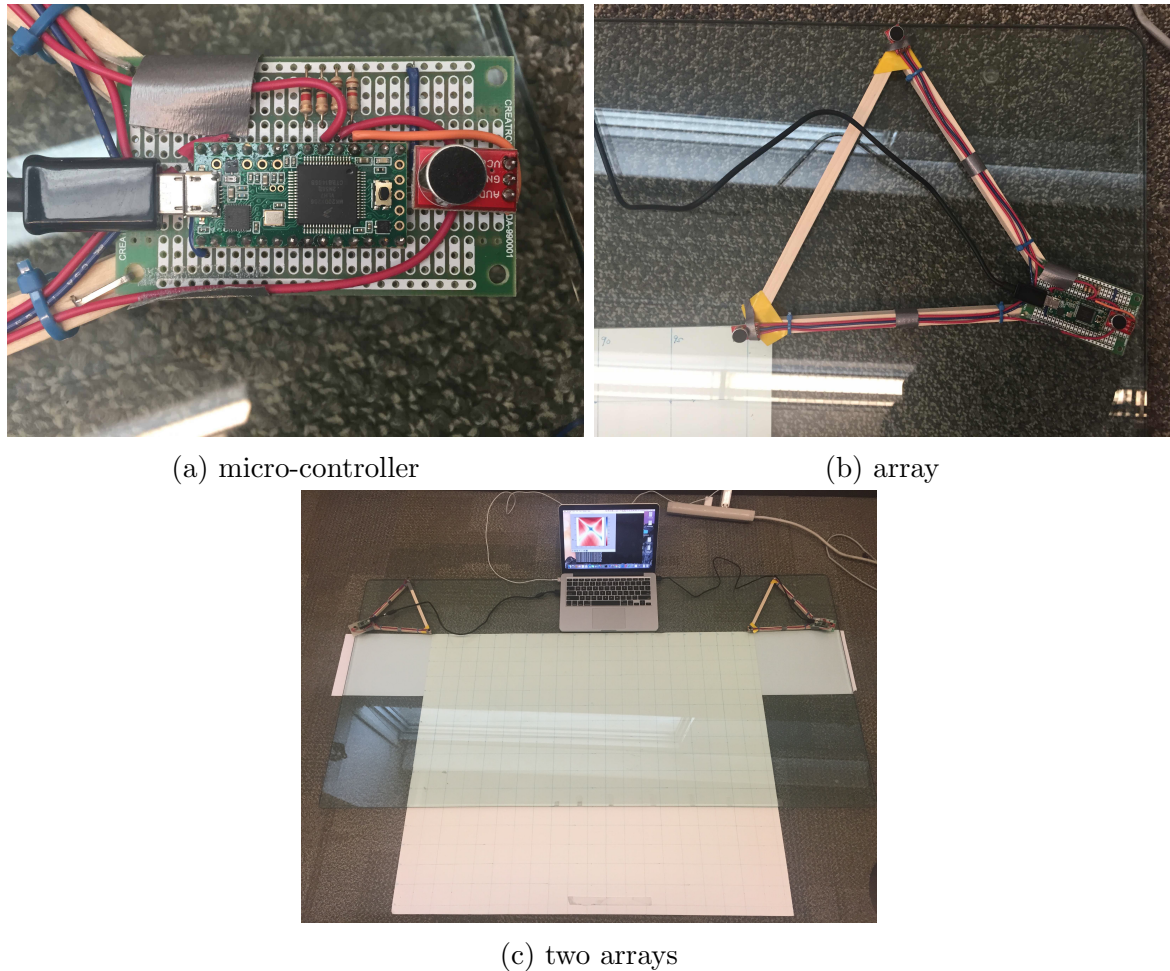


Figure 4.1: Localization system setup

can be built by superposing the likelihood from each microphone pair:

$$\begin{aligned} L(x, y) = & R_{m_1, m_2}(D_{m_1, m_2}(x, y)) + R_{m_1, m_3}(D_{m_1, m_3}(x, y)) \\ & + R_{m_2, m_3}(D_{m_2, m_3}(x, y)) \end{aligned}$$

where $R_{m_1, m_2}(\tau)$, $R_{m_1, m_3}(\tau)$, and $R_{m_2, m_3}(\tau)$ denote GCC output from microphone pairs $m_1 m_2$, $m_1 m_3$, and $m_2 m_3$.

Likelihood maps from two arrays can be combined into the final likelihood map:

$$L(x, y) = L_1(x, y)L_2(x, y) \quad (4.1)$$

where $L_1(x, y)$ and $L_2(x, y)$ represent the likelihood map from array 1 and array 2.

To see the effect of accuracy improvement using multiple arrays, fig 4.2 shows a real life localization where the source is placed at (0 cm, -30 cm). It shows the individual likelihood map from each array and also the combined likelihood map according to equation 4.1. Individual arrays give accurate angle estimate, but have high uncertainty in distance estimate. The combined likelihood map demonstrated that by merging estimates from two arrays the system is able to perform more accurate localization.

From a timing point of view, the micro-controller spends 12 milliseconds on sampling the microphone data before sending it to a computer for processing. Sending the data through the USB port takes another 15 milliseconds, and processing on the computer takes around 50 milliseconds. Therefore, the total time lag between sound source and localization is around 80 milliseconds.

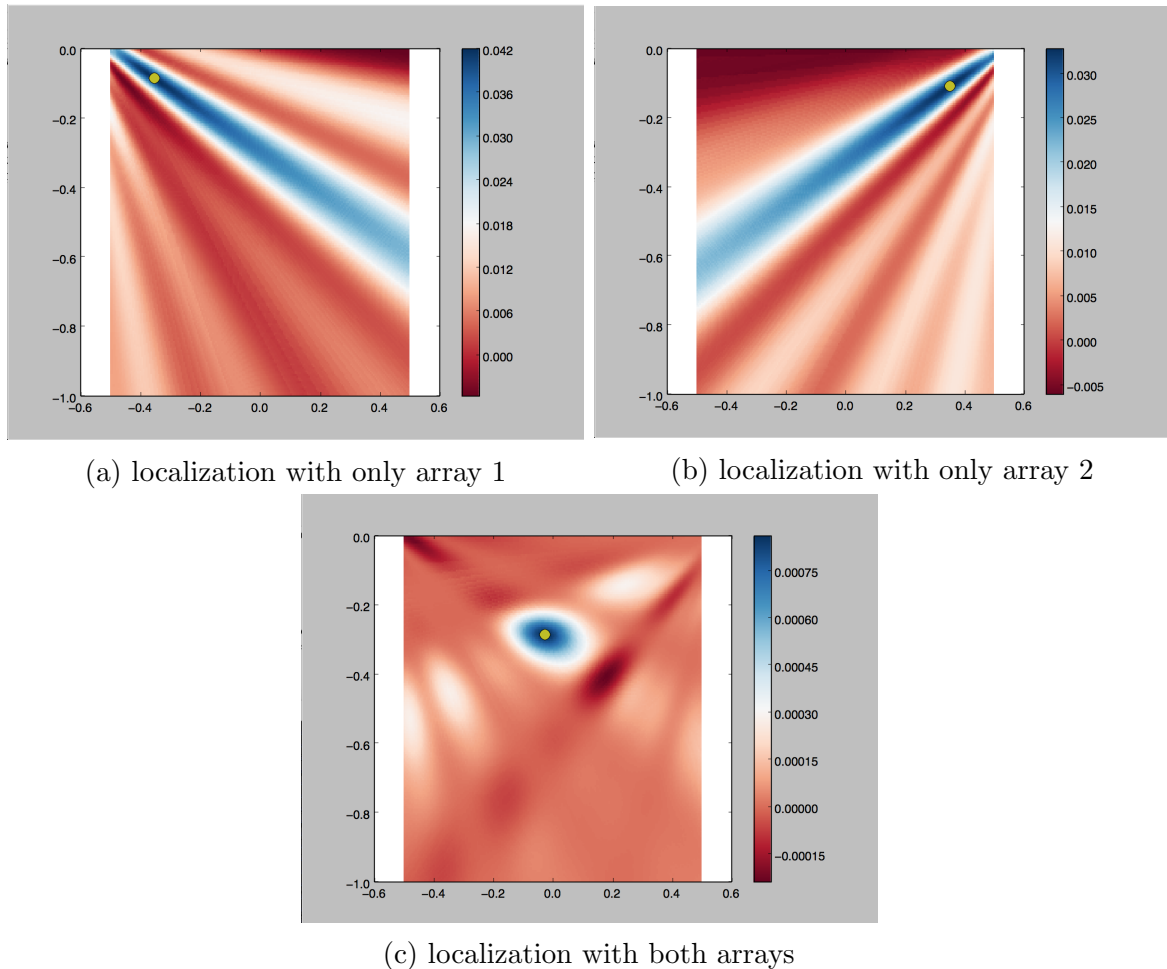


Figure 4.2: Likelihood maps for localization. The source is placed at $(0.0, -0.3)$ m

Chapter 5

Experiment

We conducted two sets of experiments to evaluate the system's localization accuracy: one on point localization and the other on movement tracking.

5.1 Setup

5.1.1 Point localization

An one meter by one meter grid was set up where the arrays were placed at the top left and top right corners of the grid. Fig 5.1 shows a picture of the setup. A total of 32 testing locations were chosen uniformly in this grid. We reported the error as the average distance between our placement of the audio source and the location estimated from the arrays.

5.1.2 Movement tracking

To test how well the system tracks movement, we mounted a rotating disk 40 centimeters in diameter onto the grid at ($x = 0$ cm, $y = -30$ cm). Fig 5.6 shows a picture of the setup. A sound source is placed on the edge of the rotating disk and the arrays track the sound source as it rotates in a circle. In this experiment, we evaluated how accuracy

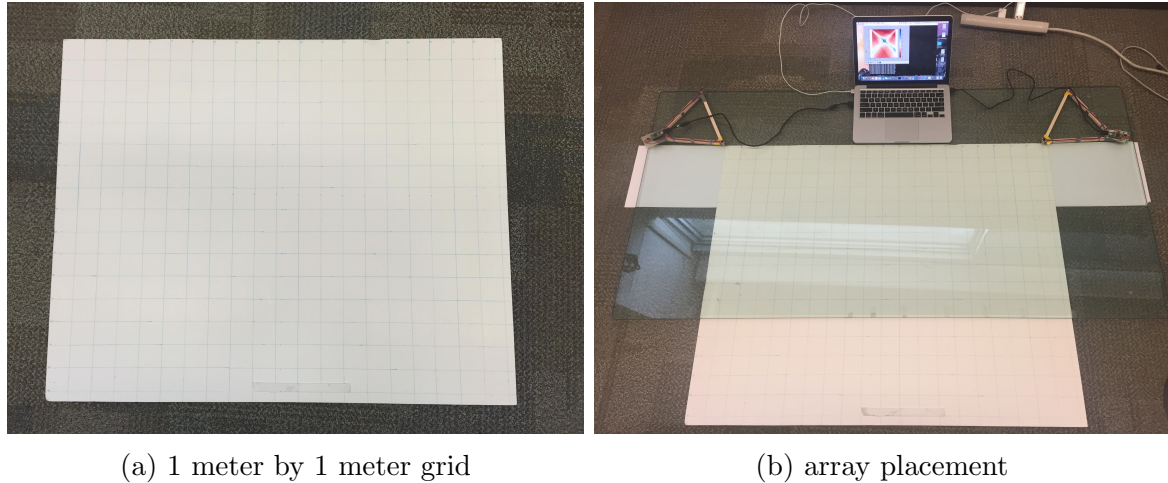


Figure 5.1: Setup for point localization evaluation

changes with:

- window sizes
- audio sources
- movement tracking filters
- movement speeds

To test how different sound sources impact localization quality, we conducted the experiments with three different sound sources:

White Noise A recording of white noise.

Music A A randomly picked music that has normal audio amplitude throughout the experiment period. *Honest Eyes* by *Black Tide* was the music used.

Music B A randomly picked music with intermittent low amplitude sections. *Canon* was the music used.

To test how the movement speed of sound source affects localization quality, each experiment was conducted at two different speeds:

Normal An angular speed of 0.5 rad/s was maintained, which translates to a linear speed of 10 cm/s.

Fast An angular speed of 1.0 rad/s was maintained, which translates to a linear speed of 20 cm/s.

For each experiment conducted, two different movement filters were evaluated:

Averaging filter localization for past 0.5 seconds were averaged and outputted as current estimate.

Kalman filter A 2nd order Kalman filter was used.

In the movement tracking experiments described above, we have the ground truth location of the circle, but not the exact location of the audio source at each moment during the movement. Therefore, the error is reported as the distance between the localized point to its closest point on the ground truth circle.

5.2 Results

5.2.1 Point localization

To test how accuracy varies with window size, the algorithm is fed with microphone data of different lengths, and the result is shown in fig 5.2. The error decreases as window size increases and plateaus after the window size exceeds around 10 millisecond. The lowest error achieved is 2.53 centimeters, which occurred when the window size is set to 12 millisecond and GCC_PPHAT is used for TDOA estimation.

Although accuracy improves with the window size, computation time also increases with it. The part of calculation that depends on the window size is using cross correlation for TDOA estimation. Cross correlation can be calculated with Fast Fourier Transform (FFT) and the runtime is of order $O(N \log N)$. We measured how the computation

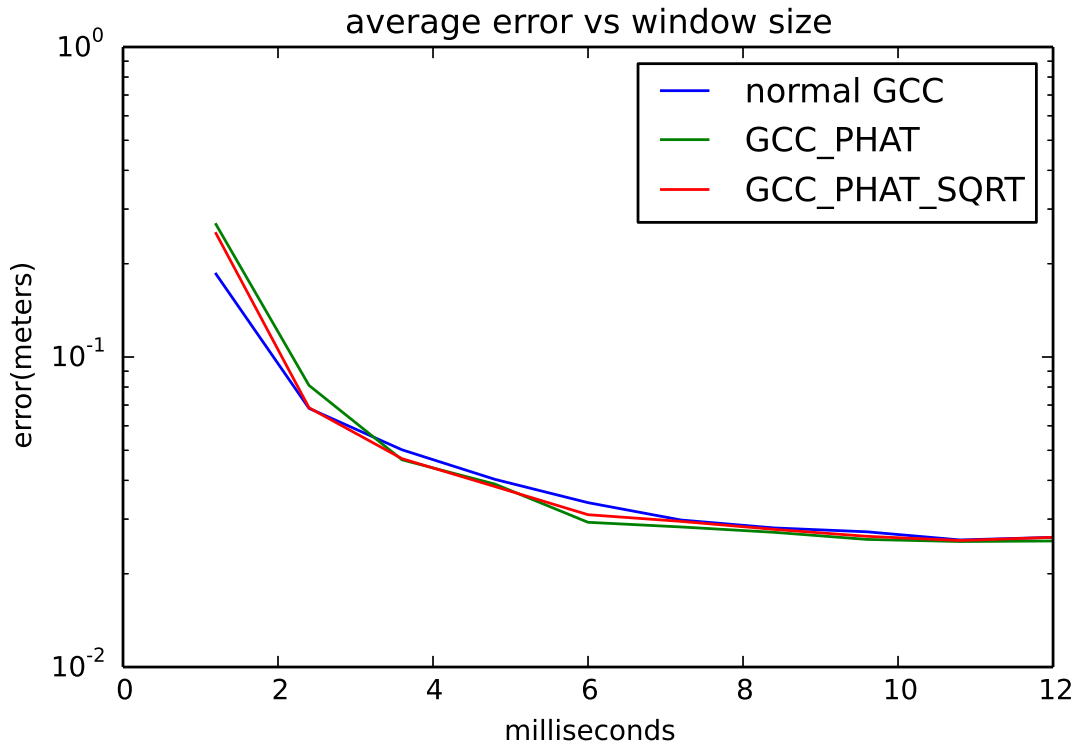


Figure 5.2: Localization error versus window size

time varied with window size and Figure 5.3 shows the result. The runtime increases approximately linearly in the window size region of interest.

We also calculated the localization error for each tested point in the grid. Figure 5.4 shows the error distribution inside the grid. The error is below 3 cm for most areas inside the grid. There is one error spike in the mid-left region and we contribute this to audio source misplacement because the error is fairly low and consistent around that spike.

To test the limit of the system and to evaluate the accuracy when the source moves outside of the one meter by one meter region, we measured the localization error by placing the source at 10 locations along y axis ranging from $(0 \text{ cm}, -10 \text{ cm})$ to $(0 \text{ cm}, -200 \text{ cm})$. The result is presented in fig 5.5. The localization error is within 3 cm when the source is within 100 cm from the arrays. The error increases to about 5 cm when the source distance increases to 150 cm and the error exceeds 10 cm after the source distance reaches 200 cm.

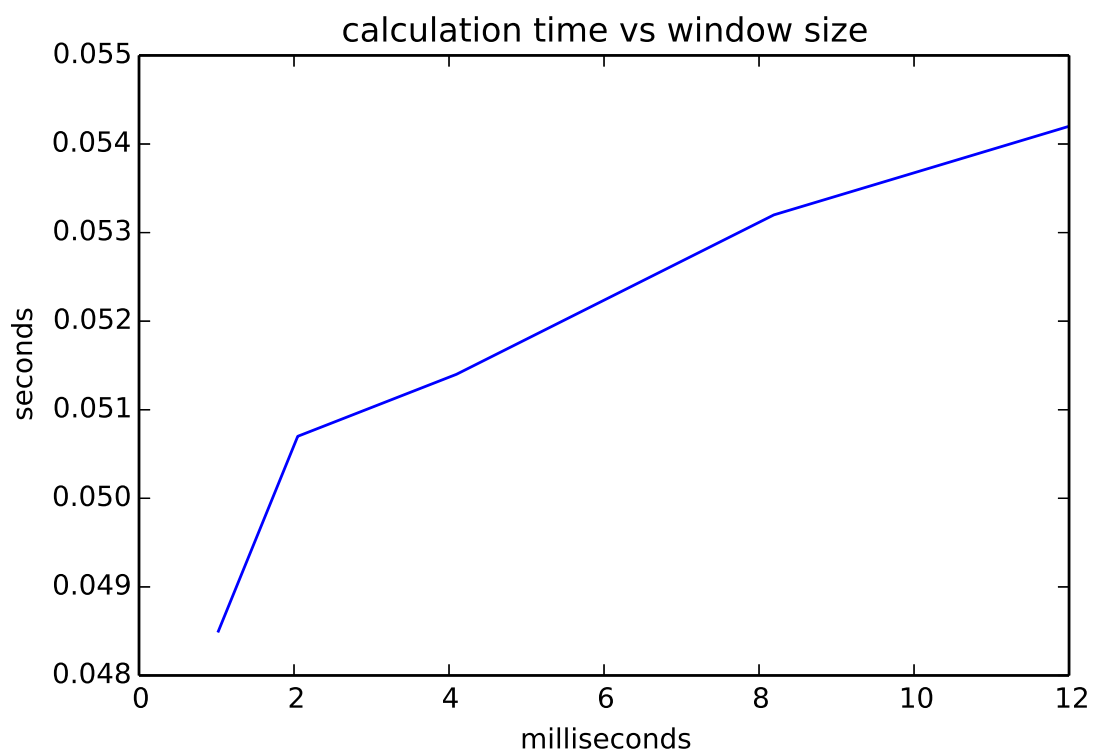


Figure 5.3: Computation time versus window size

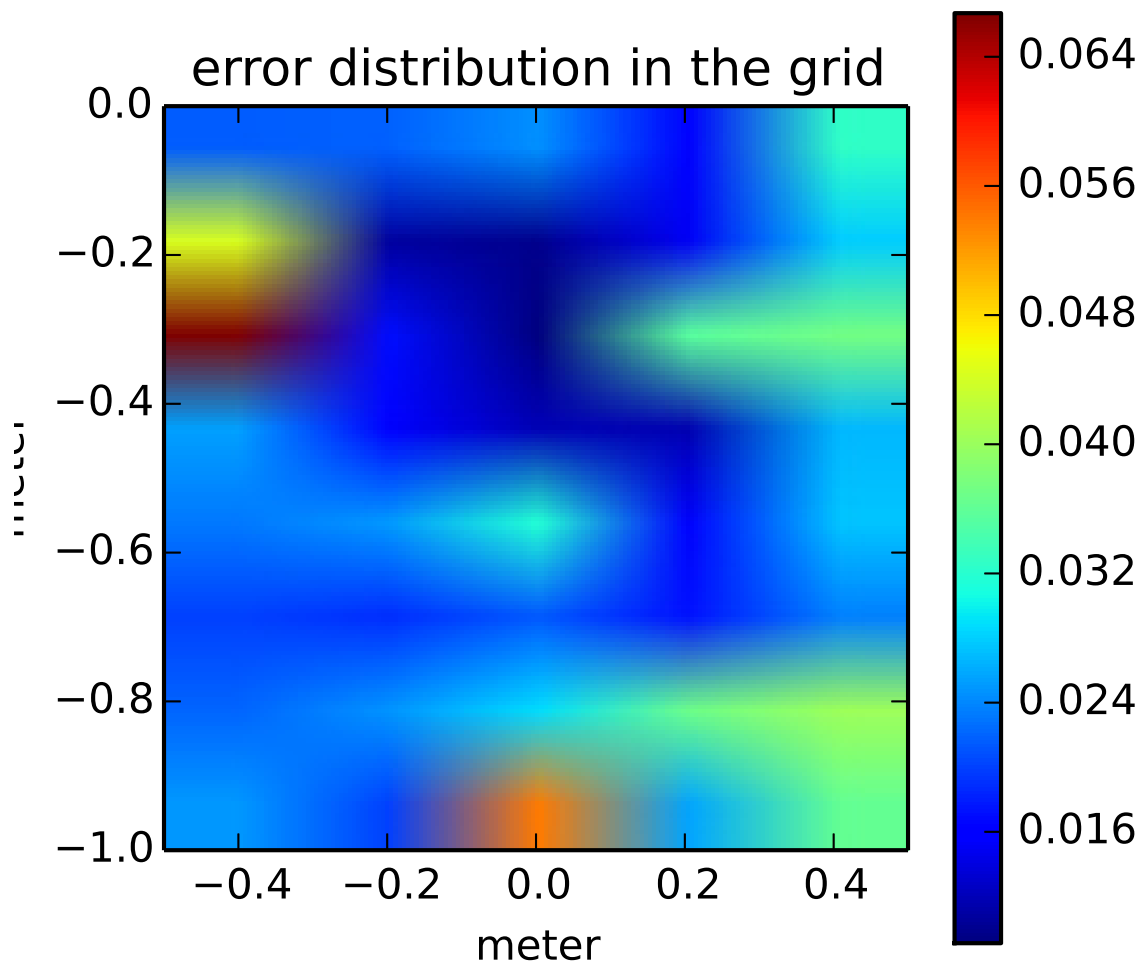


Figure 5.4: error distribution in the grid. Arrays are placed at $(-0.5 \text{ m}, 0 \text{ m})$ and $(0.5 \text{ m}, 0 \text{ m})$

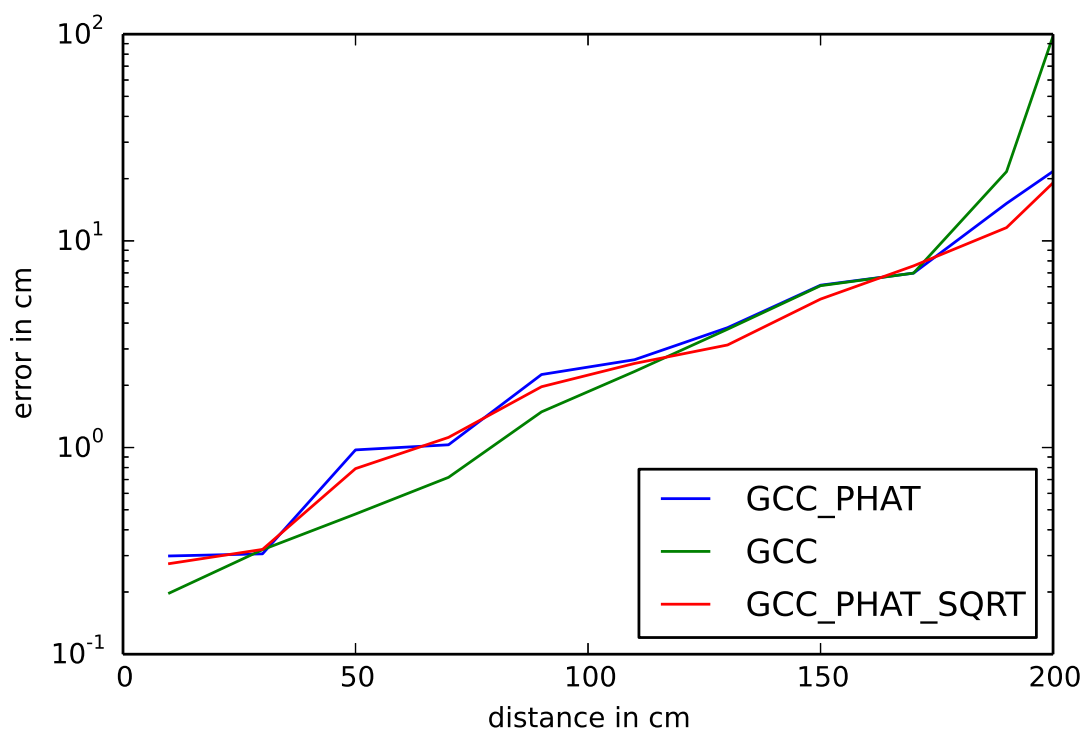


Figure 5.5: Localization error as the distance between the source and the microphone arrays increases. The source is placed on the y axis.

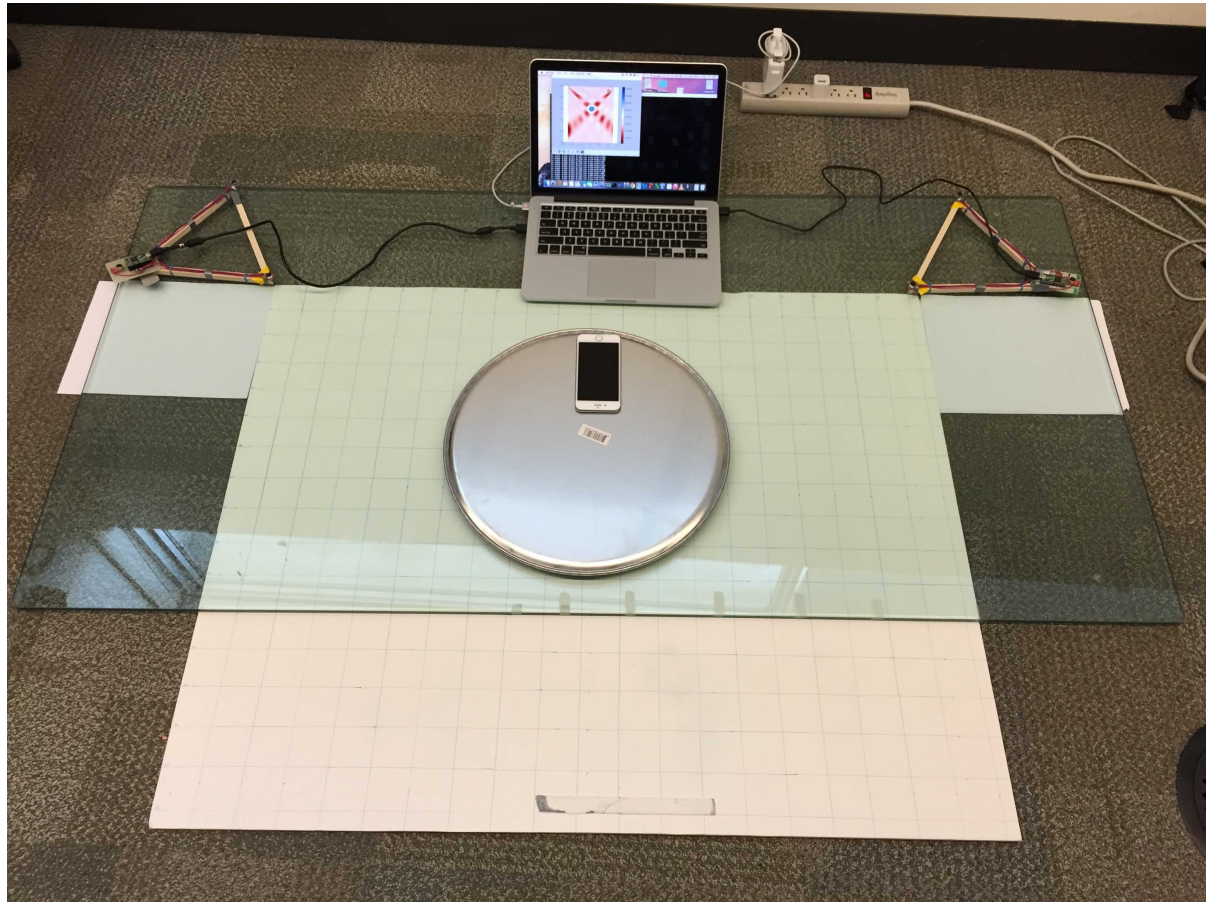


Figure 5.6: Setup for movement tracking evaluation

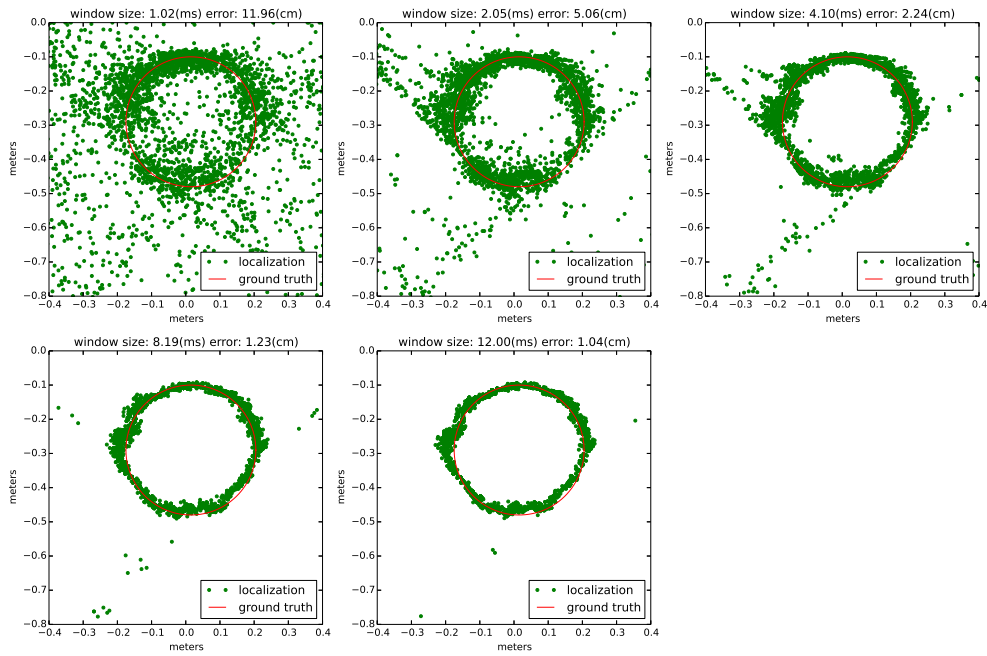


Figure 5.7: Localization quality versus window size

5.2.2 Movement tracking

Fig 5.7 gives an intuitive representation of how accuracy changes with window size. When window size is small (1.02 millisecond), the audio does not contain enough information to reliably estimate TDOA, which results in noisy localization. As window size increases, localization converges to the shape of the ground truth circle. Fig 5.8 shows how the error changes with window size. The general trend is similar to that in point localization case. Error decreases as the window size increases and plateaus after it exceeds around 10 milliseconds.

Fig 5.9 to 5.11 shows results for experiments at normal speed, and Fig 5.12 to 5.14 shows results at fast speed. By comparing localization error for each audio source between normal movement speed and fast movement speed, we find that localization error does not depend on how fast the sound source is moving. For example fig 5.10 and fig 5.13 shows that localization error is 1.289 cm at normal movement speed and 1.291 cm at fast

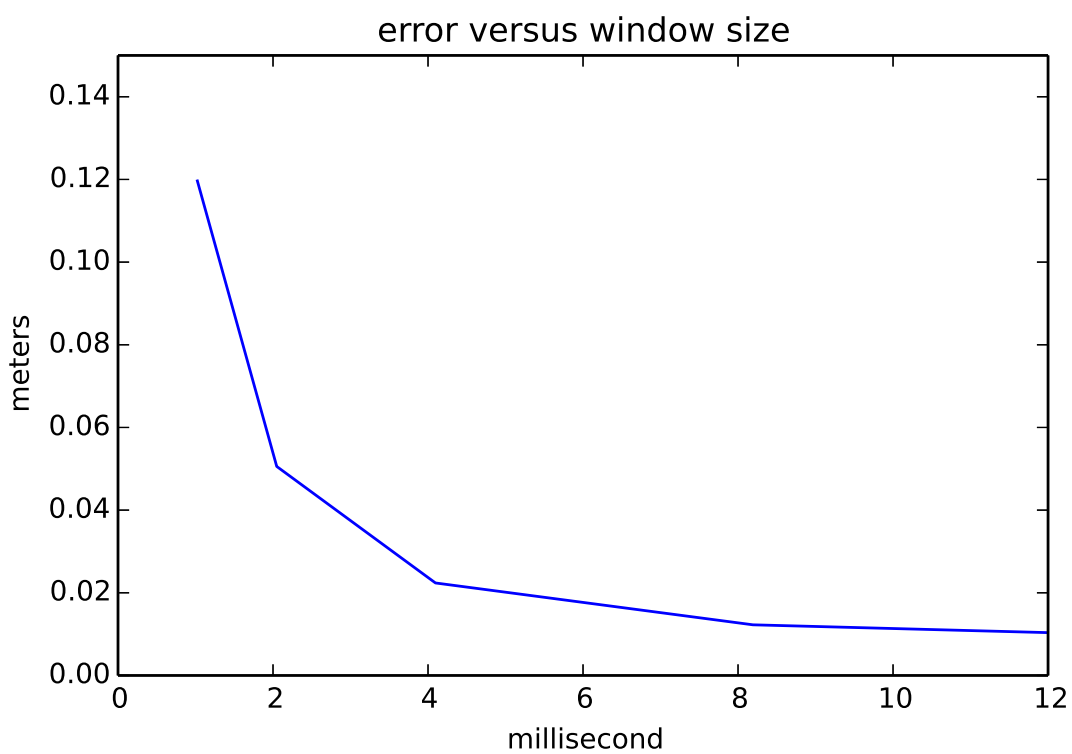


Figure 5.8: Localization error versus window size

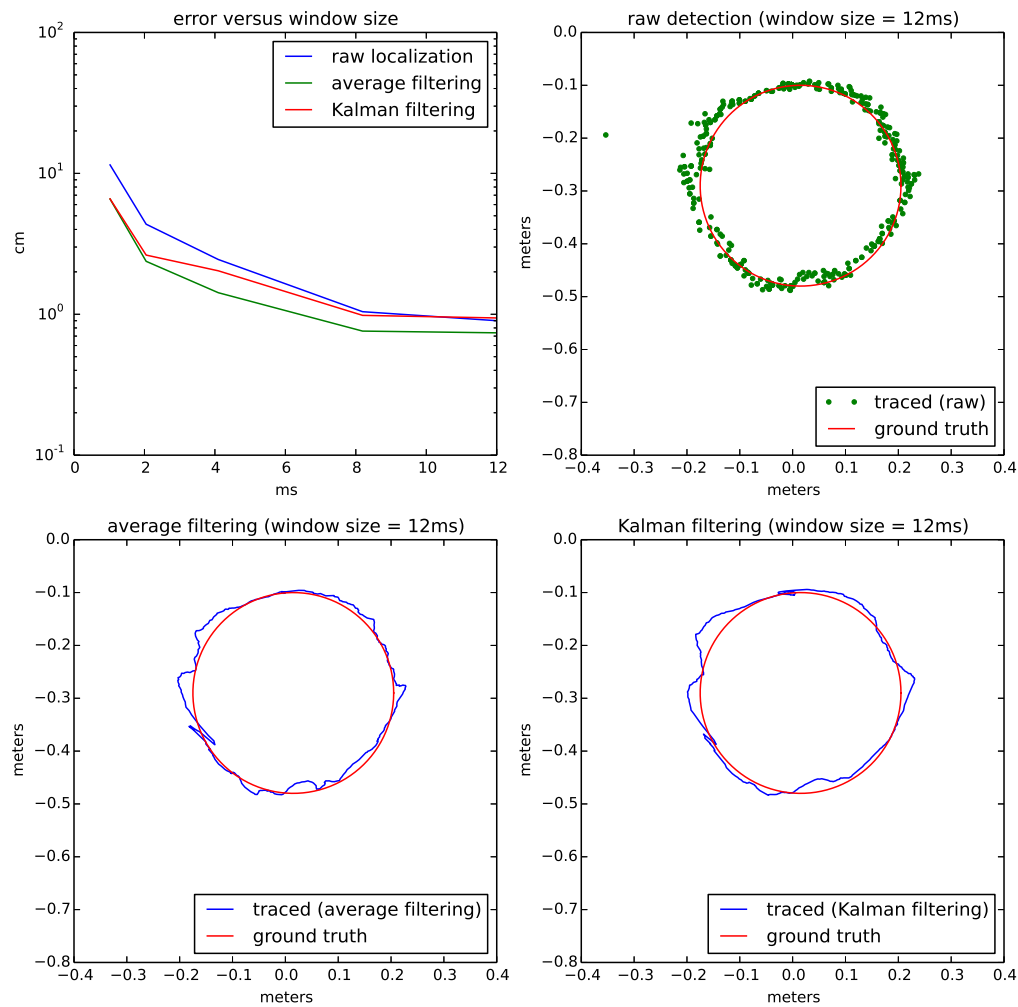


Figure 5.9: white noise (10 cm per second)

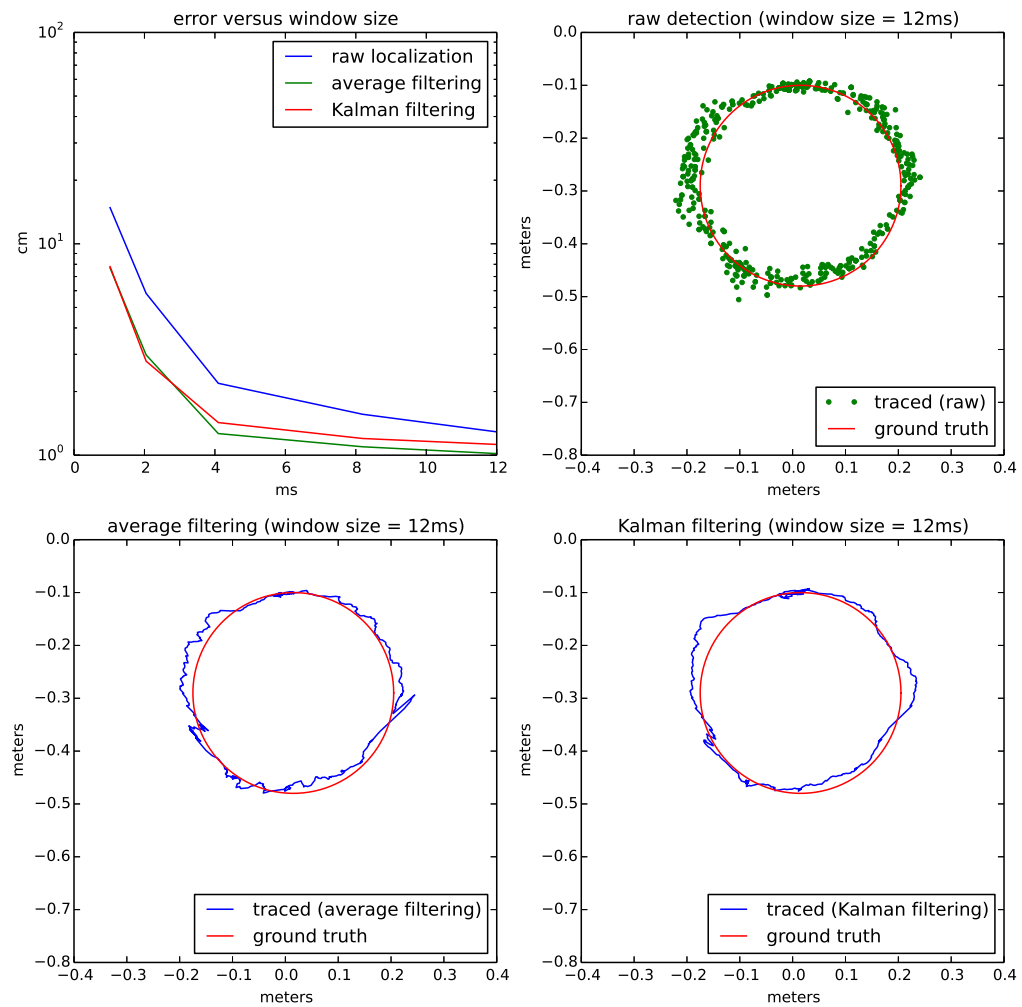


Figure 5.10: music A (10 cm per second)

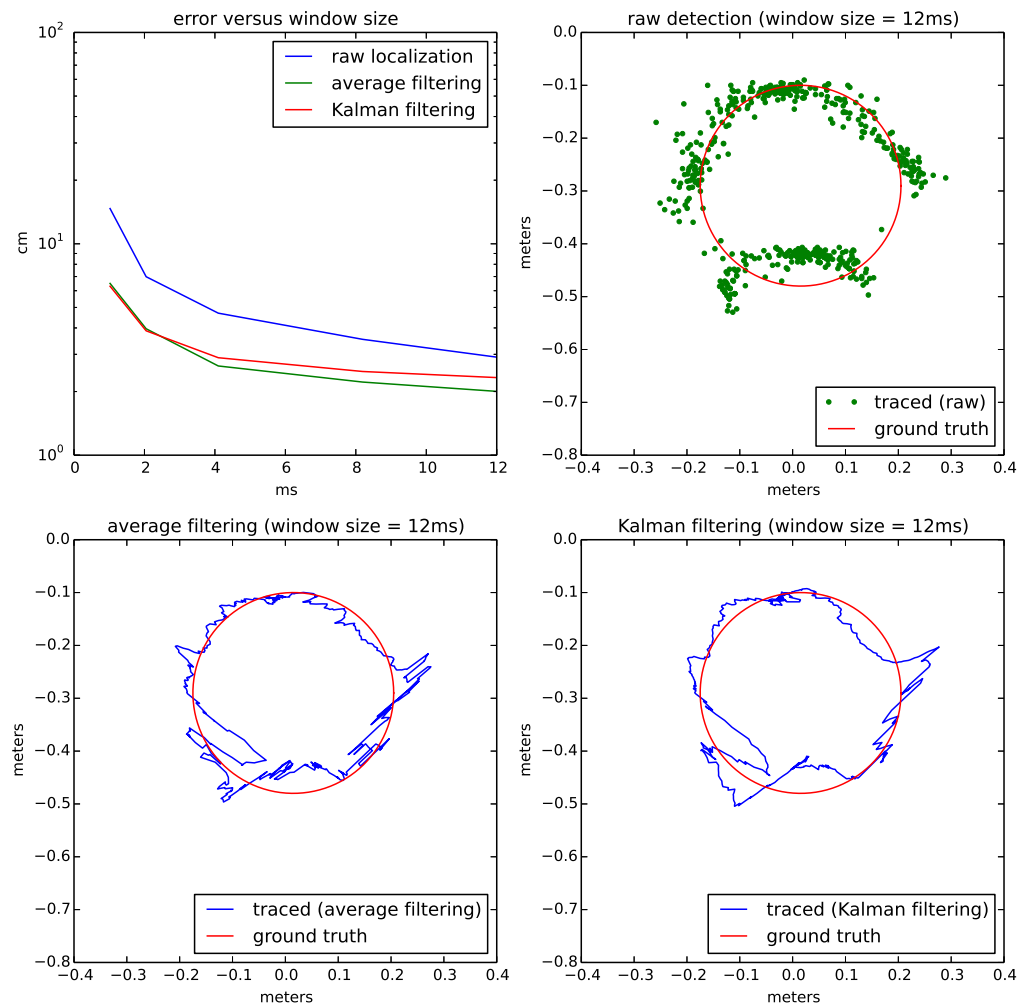


Figure 5.11: music B (10 cm per second)

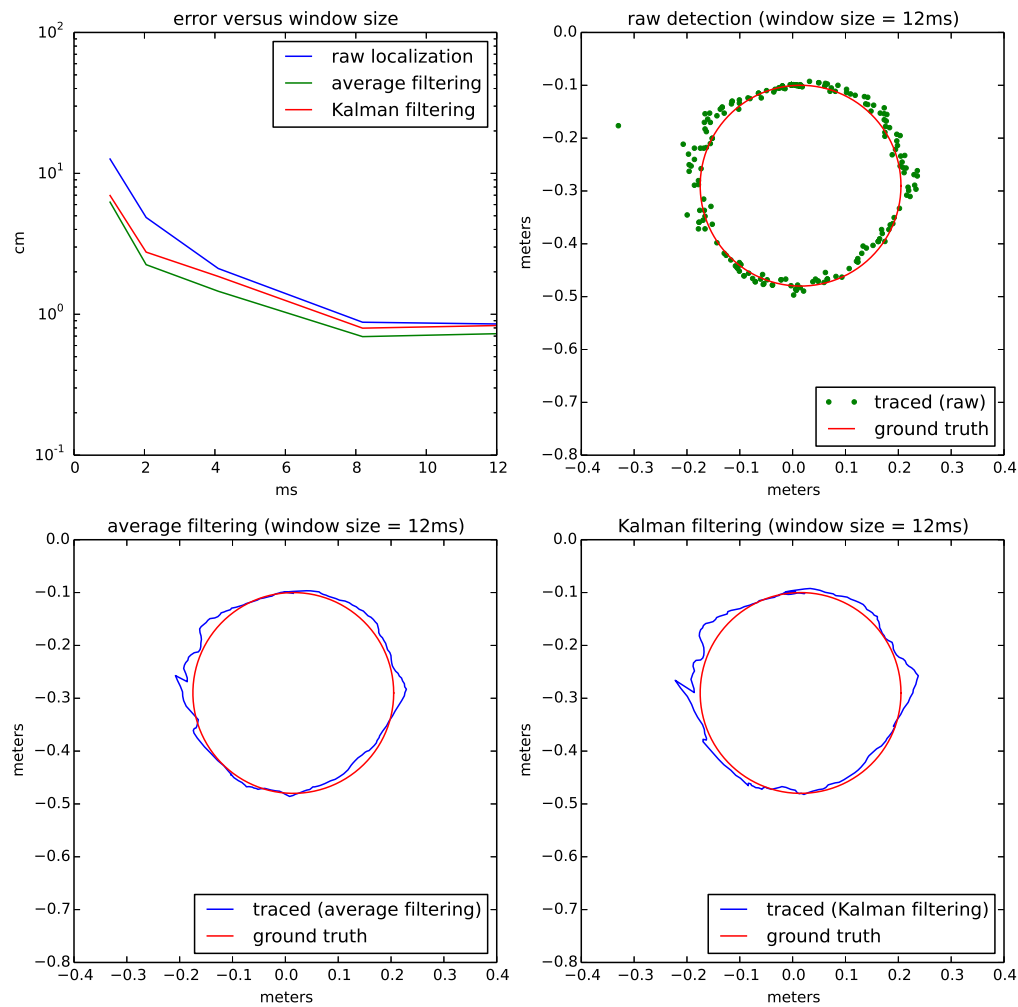


Figure 5.12: white noise (20 cm per second)

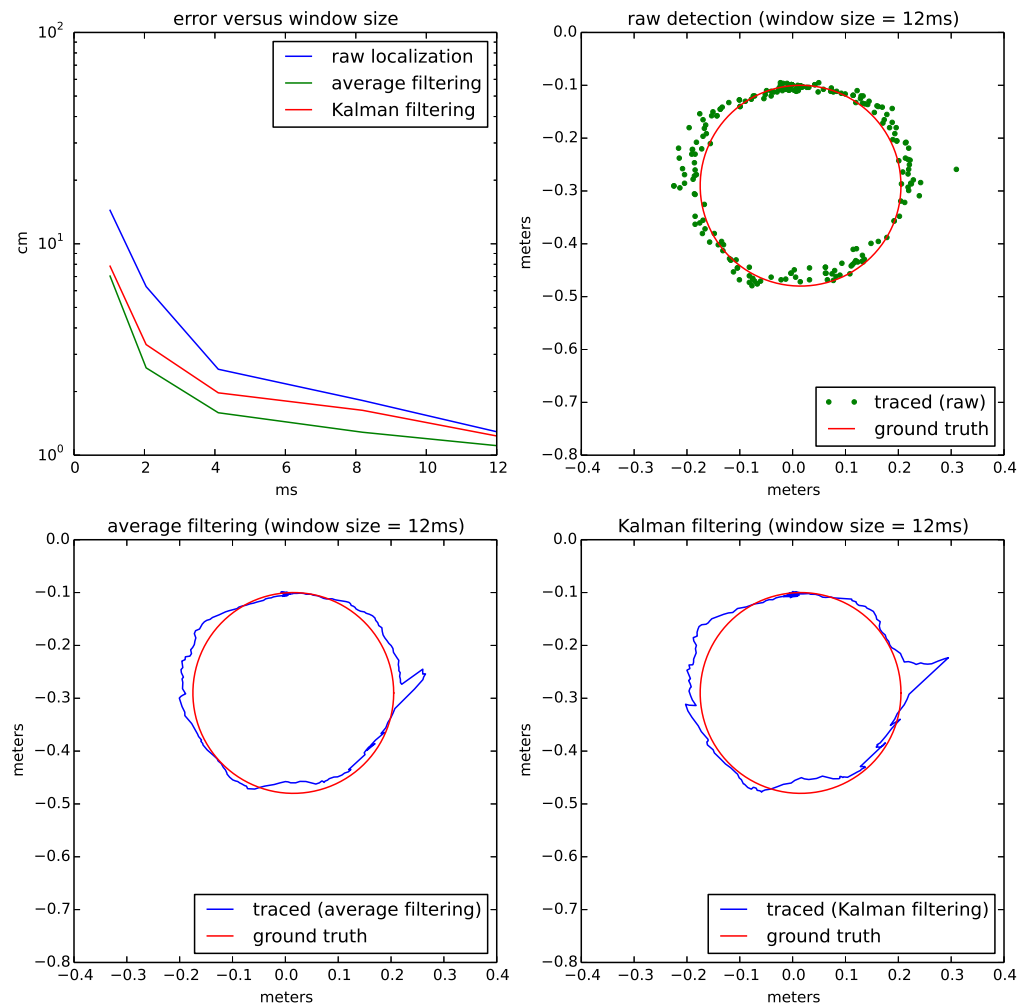


Figure 5.13: music A (20 cm per second)

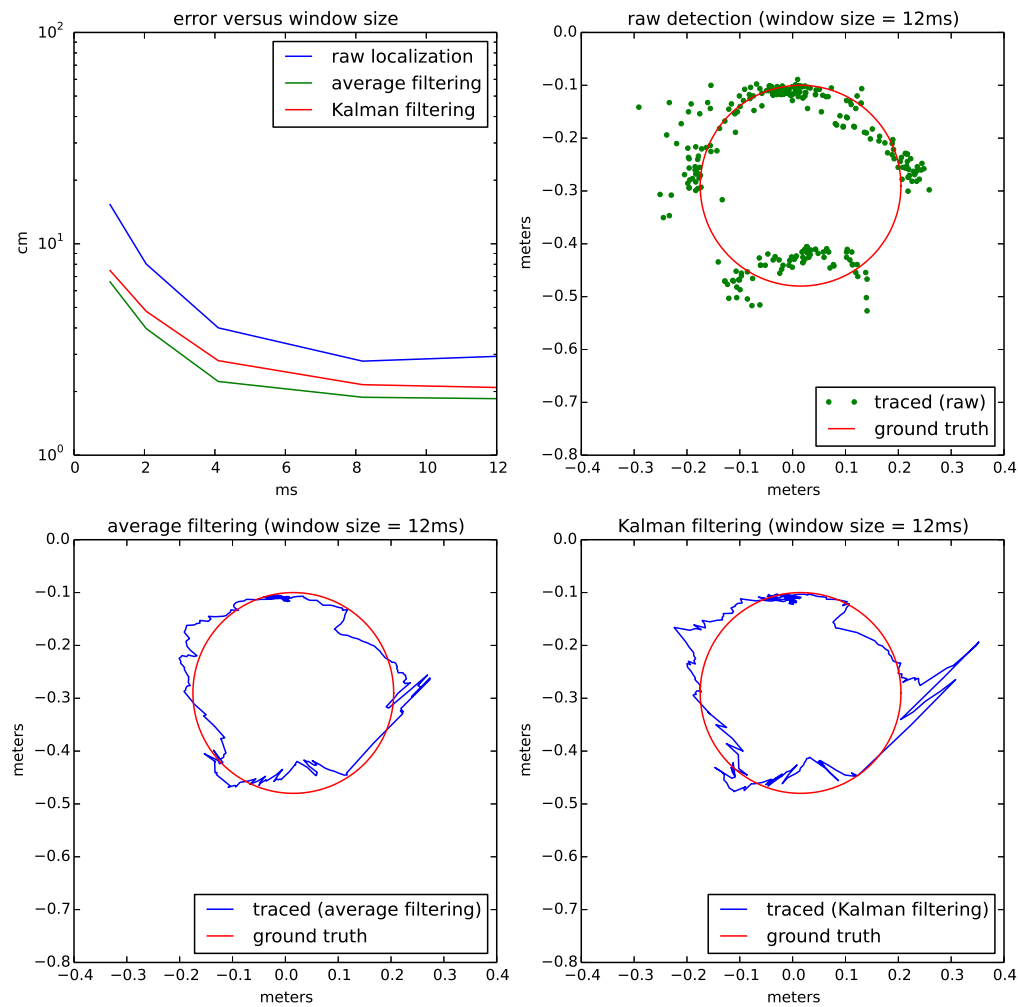


Figure 5.14: music B (20 cm per second)

movement speed.

For normal speed movement tracking, localization error is 0.9 cm for white noise, 1.29 cm for Music A, and 2.9 cm for Music B. Localization accuracy is the best for white noise source, and worst for Music B. This is consistent with our expectation because low amplitude regions in Music B would cause arrays to lose track of where the source is. This can also be seen from the “blank” regions in fig 5.11.

It also shows that raw detection has the most amount of jiggling. Kalman filter reduces the amount of jiggling from raw detection. Averaging filter has the least amount of jiggling. However, averaging filter averages detection outputs from past 0.5 seconds, which makes the filtered output lag the real movement.

Chapter 6

Conclusion

In this paper, we described and built an inexpensive, portable yet reasonably accurate sound localization system with two microphone arrays. We analyzed different array architectures and demonstrated that a two array architecture achieves better accuracy compared to a single array system of similar size. By using cross-correlation output as the likelihood for different arrival time differences, each array generates a likelihood map for each possible location in the area. We demonstrated that by merging likelihood maps from the two arrays, we were able to achieve good localization accuracy (less than 3 cm average error) in a local one meter by one meter region.

This system can be used in HCI applications that incorporate sound position and movement information, such as drawing with music, or can be used to create AI games with physical pieces where the computer controls some of the pieces. This system can also be used to in Augmented Reality (AR) applications that allow user computer interaction with music tags.

For future directions, this system can be extended with another microphone on each array to perform 3D localization. Another possible direction is to investigate multi-source localization using digitally tagged audio sources.

Bibliography

- [1] Wing, Michael G. and Eklund, Aaron and Kellogg, Loren D. “Consumer-Grade Global Positioning System (GPS) Accuracy and Reliability,” *Journal of Forestry*, 2005.
- [2] Bekkelien, Anja, Michel Deriaz, and Stphane Marchand-Maillet. “Bluetooth indoor positioning,” *Master’s thesis, University of Geneva*, 2012.
- [3] Hui Liu; Darabi, H.; Banerjee, P.; Jing Liu, “Survey of Wireless Indoor Positioning Techniques and Systems,” *IEEE Transactions on Systems, Man, and Cybernetics, Part C: Applications and Reviews*, 2007
- [4] Yazici, A.; Yayan, U.; Yucel, H., “An ultrasonic based indoor positioning system,” *2011 International Symposium on Innovations in Intelligent Systems and Applications (INISTA)*, 2011
- [5] Birchfield, Stanley T., and Rajitha Gangishetty, “Acoustic localization by interaural level difference,” *IEEE International Conference on Acoustics, Speech, and Signal Processing*, 2005
- [6] Blauert, Jens. “Spatial hearing: the psychophysics of human sound localization,” *MIT press*, 1997.

- [7] Raspaud, Martin, Harald Viste, and Gianpaolo Evangelista, “Binaural source localization by joint estimation of ILD and ITD,” *IEEE Transactions on Audio, Speech, and Language Processing*, 2010.
- [8] Chowdhury, T., Aarabi, P., Weijian Zhou, Yuan Zhonglin, and Kai Zou, “Extended touch user interfaces,” *IEEE International Conference on Multimedia and Expo (ICME)*, 2013.
- [9] Pham, D. T., et al. “Tangible acoustic interface approaches,” *Proceedings of IPROMS 2005 Virtual Conference*, 2005.
- [10] XueXin Yap, Khong, A.W.H., and Woon-Seng Gan, “Localization of acoustic source on solids: A linear predictive coding based algorithm for location template matching,” *IEEE International Conference on Acoustics Speech and Signal Processing (ICASSP)*, 2010
- [11] Chowdhury, Tusi. “Single Microphone Tap Localization,” *University of Toronto*, 2013.
- [12] Ishii, Hiroshi, et al. “PingPongPlus: design of an athletic-tangible interface for computer-supported cooperative play,” *Proceedings of the SIGCHI conference on Human Factors in Computing Systems*. ACM, 1999.
- [13] Paradiso, Joseph A., et al. “Passive acoustic sensing for tracking knocks atop large interactive displays,” *Proceedings of IEEE. Vol. 1. IEEE*, 2002.
- [14] MicLoc, URL: <http://ruralhacker.blogspot.ca/p/micloc.html>
- [15] PJRC, URL: <https://www.pjrc.com/teensy/teensy31.html>
- [16] Polotti, Pietro, et al. “Acoustic Localization of Tactile Interactions for the Development of Novel Tangible Interfaces,” *Proc. of the 8th Int. Conference on Digital Audio Effects (DAFX-05)*, 2005.

- [17] Paradiso, Joseph A., et al. “Sensor systems for interactive surfaces,” *IBM Systems Journal*, 2000.
- [18] Checka, Nisha “A system for tracking and characterizing acoustic impacts on large interactive surfaces,” *Diss. Massachusetts Institute of Technology*, 2001.
- [19] Brandstein, M.S.; Silverman, H.F., “A robust method for speech signal time-delay estimation in reverberant rooms,” *IEEE International Conference on Acoustics, Speech, and Signal Processing*, 1997.
- [20] Knapp, C. and Carter, G.Clifford, “The generalized correlation method for estimation of time delay,” *IEEE Transactions on Acoustics, Speech and Signal Processing*, 1976.
- [21] Aarabi, P. and Guangji Shi, “Phase-based dual-microphone robust speech enhancement,” *IEEE Transactions on Systems, Man, and Cybernetics, Part B: Cybernetics*, 2004.